

Journal Pre-proof

Modeling Multi-Stimuli-Responsive Shape Memory Polymers with Reduced Working Temperature

M. Baniasadi , E. Yarali , M. Bodaghi , A. Zolfagharian ,
M. Baghani

PII: S0020-7403(20)31824-5
DOI: <https://doi.org/10.1016/j.ijmecsci.2020.106082>
Reference: MS 106082



To appear in: *International Journal of Mechanical Sciences*

Received date: 27 April 2020
Revised date: 24 August 2020
Accepted date: 6 September 2020

Please cite this article as: M. Baniasadi , E. Yarali , M. Bodaghi , A. Zolfagharian , M. Baghani , Modeling Multi-Stimuli-Responsive Shape Memory Polymers with Reduced Working Temperature, *International Journal of Mechanical Sciences* (2020), doi: <https://doi.org/10.1016/j.ijmecsci.2020.106082>

This is a PDF file of an article that has undergone enhancements after acceptance, such as the addition of a cover page and metadata, and formatting for readability, but it is not yet the definitive version of record. This version will undergo additional copyediting, typesetting and review before it is published in its final form, but we are providing this version to give early visibility of the article. Please note that, during the production process, errors may be discovered which could affect the content, and all legal disclaimers that apply to the journal pertain.

© 2020 Elsevier Ltd. All rights reserved.

Highlights

- Modeling fibrous thermo-electro-magneto-responsive shape memory polymers
- Reinforcing SMPs by using electro-magnetic fields and embedding fibers
- Reducing the working temperature of SMPs to make them more bio-applicable
- Semi-analytical solution of the model under extension and torsion-extension loadings

Journal Pre-proof

Modeling Multi-Stimuli-Responsive Shape Memory Polymers with Reduced Working Temperature

M. Baniasadi ^{a,1}, E. Yarali ^{a,1}, M. Bodaghi ^{b*}, A. Zolfagharian ^c and M. Baghani ^a

^a School of Mechanical Engineering, College of Engineering, University of Tehran, Tehran, 11155-4563, Iran

^b Department of Engineering, School of Science and Technology, Nottingham Trent University, Nottingham NG11 8NS, United Kingdom

^c School of Engineering, Deakin University, Geelong 3216, Australia

1 P.E. M. Baniasadi and E. Yarali contributed equally to this work as first authors.

* Corresponding Author, Email Address: mahdi.bodaghi@ntu.ac.uk ; Tel.: +44-115-84-83470

Abstract

Nowadays, shape memory polymers (SMPs)-based devices are required to be much smarter to produce large shape memory recovery and recovery force with lower working temperatures. They could play a vital role in the advancement of soft robot manipulators, biomedical tools and wearable devices where the working temperatures is a key challenge and must be around the body temperature, or in sustainable smart systems with low energy consumption. The aim of this paper is to introduce thermo-electro-magneto-responsive fibrous SMPs (TEMFSMPs) as a new class of SMPs with highly enhanced shape recovery and recovery force and reduced working temperature. A three-dimensional constitutive model is developed to simulate thermo-electro-magneto-visco-hyperelastic behaviors of SMPs under large deformation for the first time. Constitutive relations are derived by adopting an electro-magneto-visco-hyperelasticity theory and implementing it in a thermo-mechanical cycle of SMPs. To improve the strength of thermo-electro-magneto-responsive SMPs, a bunch of fibers is also embedded into the SMP matrix. Then, the proposed model for thermo-electro-magneto-responsive fibrous shape memory polymers (TEMFSMPs) under uniaxial tension and complex loading regimes such as simultaneous torsion and extension are solved semi-analytically. In addition, the thermo-mechanical response through the proposed model is validated via available SMP experimental tests. Numerical results reveal that electro-magnetic features can significantly enhance shape memory recovery and recovery force of TEMFSMPs and lower their working temperatures. It is found that the electro-magnetic field, the orientation, and stiffness of fibers can effectively be set to tune the shape memory effect and bio-applicability of TEMFSMPs with highly enhanced stress/strain recovery and reduced working temperature.

Keyword: *Multi-Stimuli-Responsive Polymers; Constitutive modeling; thermo-electro-magneto-visco-hyperelasticity; fiber-reinforced shape memory polymers; large deformation; semi-analytical solution.*

1 Introduction

As an emerging class of smart polymers, shape memory polymers (SMPs) feature the ability to recover their permanent shapes from one (or multiple [1, 2]) programmed temporary shape(s) when exposed to specific stimuli, such as heat [3-5] electricity [6, 7], light [8, 9], magnetic fields [10, 11] and solvents [12]. Also, they can work in one cycle, called one-way SMPs or several reversible cycles, called two-way SMPs [13]. Compared with shape memory alloys, SMPs possess the advantages of high strain recovery (up to 1000% [14]), low density, low cost, biocompatibility and easy shape-programming process [15]. SMPs due to their Shape Memory Effect (SME) and self-healing property are designed into actuators or sensors offering outstanding advantages and extensively utilized in various fields such as aerospace, biomedical, civil engineering, and 3D (or 4D) printing [16-22]. Among different stimuli, heat is the most common to stimulate SMPs. Besides, heat can be generated in direct and indirect ways (*e.g.*, inducing heat remotely). Considering the open literature, there are a lot of constitutive models for thermally-induced SMPs under small and large strains [22]. For other types of SMPs (*e.g.*, electro-magneto-responsive SMPs), however, there is only one model for electro-responsive SMPs [23]. Thermally-induced SMPs have some disadvantages. One of them is their softening effect due to the temperature rise. It means that, under heating recovery step when the temperature of SMPs is being more than their glass transition temperature, SMPs stiffness dramatically decreases. This disadvantage mostly restricts the application of SMPs in soft robotics and manipulators in which using nanocomposites is a method to improve the SMP recovery force [24, 25]. Another one is that in some applications such as biomedical devices, working temperature of SMPs must be around body temperature. However, most thermally-induced SMPs have working temperatures higher than the body temperature. To settle these issues, other stimuli-responsive SMPs can be more satisfying alternatives. In this respect, electro- or magneto-responsive SMPs or electro-magneto-responsive SMPs have been developed due to their remotely actuation and stiffening effect.

Electro-magneto-rheological elastomers (EMREs) can be categorized as another class of smart materials that are capable of changing their electric, magnetic and mechanical properties in the presence of electric, magnetic and mechanical fields [26]. In fact, in electro-rheological or magneto-rheological materials including fluids or polymers, ferromagnetic or electric particles are oriented parallel to applied fields while being triggered by electric, magnetic, or their coupling [27]. Adding electro-active particles such as carbon nanotubes

and magneto-active particles such as Fe_3O_4 or carbonyl iron to elastomers makes the matrix multi-trigger EMREs. Thanks to their unique properties, they have found great potential in many engineering applications such as multi-trigger soft actuators [28]. Electric and magnetic fields are used to activate SMPs and EMREs in two different ways. While electric and magnetic fields induce heating into SMPs and activate the shape recovery, these fields change strength properties of EMREs. In recent years, a world-wide activity has been devoted to simulating behaviors of SMPs and EMREs. More details in constitutive modeling SMPs and EMREs can be found in research works done by Yarali et al. [22] and Rossi et al. [29]. As the understanding of SMP properties is getting deeper and deeper in material research community, the list of applications continues to expand. It has been found that SMP-based soft actuators are required to produce larger shape recovery and recovery force for practical applications like artificial muscles [30]. As mentioned before, several strategies have been introduced to increase the shape recovery and recovery force in SMPs. A preliminary work to enhance SME of SMPs is SMP composites through short fibers [25, 31], coiled carbon nanotubes (CCNTs) [24], ZnO nanoparticles [25], multi-directional circular braided tube [32]. In this way, more specifically, Yarali et al. [24] investigated the effect of different geometrical parameters of CCNTs (*e.g.*, spring length scale, pitch, and mean diameter), their volume fractions and directions. They showed that by increasing volume fraction of CCNTs up to 0.6%, the effective recovery force of the SMP is increased by 15% or the effective recovery force can be increased up to 25% utilizing adjusting CCNT's distributions. Zhang et al. [32] introduced circular braided tube preforms and the preform/silicone elastomer matrix composites to enhance the shape memory behavior and recovery force in SMPs. The effects of braiding angle, tube wall thickness, and shape recovery temperature on the shape memory behavior of tube preforms and their silicone elastomer matrix composites were found to be significant. In addition, Liu et al. [33] showed that reinforcing thermally-induced SMPs with carbon nanotubes can improve the recovery force up to 144%. They also found that the infusion of the silicone matrix can increase the final shape recovery ratio to 97.3%, improve the recovery force, and enhance the flexural property. In some other approaches, by adapting rational designs and changing the geometry of structures, the SME of SMPs may be enhanced [34].

In the field of electro- or magneto-responsive SMPs, there are some numerical and experimental research works which are briefly introduced here. For the first time, recently, a constitutive model for electro-responsive SMPs under large deformation was developed by Niyonzima et al. [23]. They developed a 3D model employing a multiphysics coupling of

thermal, electric, and mechanical phenomena and eventually discretized and solved it using a finite element approach, and finally implemented it for the application of stents. In an experimental work, a magneto-responsive SMP including a crosslinked poly(dimethylsiloxane) (PDMS) porous matrix and magnetorheological fluid drops was introduced by Testa et al. [11]. They tested the proposed SMP under different loading regimes and found it fully reversible and fast response. In addition, there are several research works led by Leng's group on electro-responsive SMPs including carbon nanotubes (CNTs) [7] and magneto-responsive Fe_3O_4 -based SMPs [35] and by Calvo-Correas et al. [36] on magneto-responsive SMPs including synthesized magnetic nanoparticles. They showed that increasing the volume fraction of additives not only makes the pure SMP much stiffer and eventually changes the glass transition temperature of the SMP, but also the additives keep the surface temperature of the SMP around 40°C which is useful for biomedical applications.

As mentioned previously, two key challenges of thermally-induced SMPs, especially for biomedical applications, are the softening effect induced during the recovery stage, and their high working temperature which restrict their applicability when used in the body. The literature review reveals that there are no constitutive models for thermo-electro-magneto-responsive SMPs. The aim of this paper is to introduce a novel class of SMPs so-called thermo-electro-magneto-responsive fibrous SMPs (TEMFSMPs) with highly enhanced shape recovery and recovery force and reduced working temperature, see Figure 1 for inspiration. The strength of thermo-electro-magneto-responsive SMPs is improved by coupling different fields and embedding a bunch of fibers into the matrix. A 3D constitutive model is developed for TEMFSMPs based on the non-linear electro-magneto-visco-hyperelasticity theory. The proposed model is then considered for the cases of uniaxial tension and simultaneous torsion and extension loading regimes and solved semi-analytically. A comparison between semi-analytical results and experimental data available in the literature for thermally-responsive pure SMPs is conducted verifying the accuracy of the model and solution methodology. Finally, the effects of some parameters such as purely electric field, purely magnetic field, electro-magnetic fields, the stiffness of fibers, and their orientation are investigated. Numerical results reveal that these parameters can be tuned to significantly enhance shape memory recovery and recovery force of TEMFSMPs and lower their working temperatures. Due to the absence of similar concepts and constitutive models in the specialized literature, this paper is likely to advance the state of the art SMPs and provide pertinent insights that are instrumental in the design of SMP devices for remote applications such as robot arms, artificial muscles, and tissue scaffolds.

This paper is organized as follows. In section 2.1, constitutive equations for thermo-visco-hyperelastic materials are introduced. Then, in section 2.2 and two sub-sections 2.2.1 and 2.2.2, the constitutive equations for fibrous electro-magneto-responsive polymers are presented. Transversely isotropic hyperelastic materials and electro-magneto-responsive theory are expressed in sections 2.2.1 and 2.2.2, respectively. Based on the elastic stress associating with electro-magneto-hyperelastic fibrous response, the total Cauchy stress is calculated in section 2.2. Then, in section 2.3, the proposed model is time-discretized. In section 3, a non-linear continuum framework of a uniaxial tension problem is proposed. In section 4.1, results and relevant discussions for the uniaxial tension are presented investigating the effects of different parameters such as purely electric field, purely magnetic field, electro-magnetic fields, the stiffness of fibers, and their orientation on the shape memory features of TEMFSMPs. Also, in section 4.2, the proposed model is solved semi-analytically under simultaneous torsion and extension loading regime. Concluding remarks are finally presented in section 5.

2 Constitutive Modeling of TEMFSMPs

2.1 Constitutive Equations for Thermo-Visco-Hyperelastic Materials

In time-dependent materials, it is a realistic assumption that the total stress can be separated into mechanical deformation and time. Based on the insight from this assumption, the generalized constitutive equation of time-dependent materials for stress relaxation tests is commonly represented as [37]:

$$\boldsymbol{\sigma}(\boldsymbol{\varepsilon}, t) = \boldsymbol{\sigma}_0(\boldsymbol{\varepsilon})\Gamma(\boldsymbol{\varepsilon}, t) \quad (1)$$

in which $\boldsymbol{\sigma}$, $\boldsymbol{\varepsilon}$, t , $\boldsymbol{\sigma}_0$ and Γ represent total stress, total strain, time, the stress associated with the instantaneous response of the material and a non-dimensional function to describe the relaxation phenomenon which is normally represented by Prony series as:

$$\Gamma(\boldsymbol{\varepsilon}, t) = \Gamma_\infty(\boldsymbol{\varepsilon}) + \sum_{i=1}^n \Gamma_i(\boldsymbol{\varepsilon}) \exp\left(\frac{-t}{\tau_i}\right) \quad (2)$$

where Γ_∞ and Γ_i ($i=1:n$) are dimensionless functions that identify the contribution of equilibrium (*i.e.*, elastic) and non-equilibrium (*i.e.*, viscous), respectively, and τ_i stands for the relaxation times of the viscous part.

Substituting Eq. (2) into Eq. (1) results in [37]:

$$\boldsymbol{\sigma}(\boldsymbol{\varepsilon}, t) = \boldsymbol{\sigma}_0(\boldsymbol{\varepsilon}, t) \left(\Gamma_\infty + \sum_{i=1}^n \Gamma_i \exp\left(\frac{-t}{\tau_i}\right) \right) = \underbrace{\boldsymbol{\sigma}_0(\boldsymbol{\varepsilon}) \Gamma_\infty(\boldsymbol{\varepsilon})}_{\text{Equilibrium Part}} + \underbrace{\boldsymbol{\sigma}_0(\boldsymbol{\varepsilon}) \sum_{i=1}^n \Gamma_i(\boldsymbol{\varepsilon}) \exp\left(\frac{-t}{\tau_i}\right)}_{\text{Viscous Part}} = \boldsymbol{\sigma}^e + \boldsymbol{\sigma}^v \quad (3)$$

Eq. (3) reveals that the total stress in time-dependent materials is composed of two terms. The equilibrium term (*i.e.*, $\boldsymbol{\sigma}^e$) is deformation-dependent and may be obtained from linear (or non-linear) elastic theory. The second term represents the stress induced by viscous properties of the material (*i.e.*, $\boldsymbol{\sigma}^v$). In fact, Eq. (3) shows that to simulate visco-hyperelastic materials, we can use a rheological model constituting two parallel parts including hyperelastic part and viscous part. More explicitly, to obtain parameters associated with time-dependent behavior of the material (*e.g.*, Γ_∞ , Γ_i and τ_i), a rheological model so called Generalized Maxwell-Kelvin is employed. To this end, its corresponding shear modulus can be written as [38]:

$$G(t) = G_\infty + \sum_{i=1}^n G_i \exp\left(\frac{-t}{\tau_i}\right) = G_0 - \sum_{i=1}^n G_i \left(1 - \exp\left(\frac{-t}{\tau_i}\right) \right) \quad (4)$$

in which G , G_∞ , G_i and G_0 stand for total shear modulus, long-term or equilibrium shear modulus, shear modulus in i -th branch of Generalized Maxwell-Kelvin model and instantaneous shear modulus which is equal to $G_\infty + \sum_{i=1}^n G_i$. Thus, the parameter of Γ_i can be expressed as G_i/G_0 .

In addition, based on the instantaneous shear modulus defined, Eq. (2) can be rewritten in another form as:

$$\Gamma(\boldsymbol{\varepsilon}, t) = 1 - \sum_{i=1}^n \Gamma_i(\boldsymbol{\varepsilon}) \left(1 - \exp\left(\frac{-t}{\tau_i}\right) \right) \quad (5)$$

As mentioned before, Eq. (1) is only used for stress relaxation tests. Therefore, the general form of Eq. (1) based on the linear viscoelastic theory in a convolution integral form and by additive decomposition it into elastic and viscous parts can be expressed as:

$$\boldsymbol{\sigma}(\boldsymbol{\varepsilon}, t) = \Gamma_\infty(\boldsymbol{\varepsilon}) \boldsymbol{\sigma}_0(\boldsymbol{\varepsilon}) + \sum_{i=1}^n \int_{-\infty}^t \frac{\partial}{\partial \zeta} (\Gamma_i(\boldsymbol{\varepsilon}) \boldsymbol{\sigma}_0(\boldsymbol{\varepsilon})) \exp\left(-\frac{t-\zeta}{\tau_i}\right) d\zeta = \boldsymbol{\sigma}^e + \boldsymbol{\sigma}^v(t) \quad (6)$$

Another form of Eq. (6) can be written as [39, 40]:

$$\boldsymbol{\sigma}(\boldsymbol{\varepsilon}, t) = \int_0^t \Gamma(t-\zeta) \frac{\partial \boldsymbol{\sigma}^e}{\partial \zeta} d\zeta \quad (7)$$

Now, to consider the effect of temperature on viscoelastic properties of amorphous polymers (*i.e.*, modeling stiffening effect while changing temperature), the time-temperature superposition principle (TTSP) is employed. In this way, the reduced time, t_r , is defined and

the thermal effect is considered by replacing the real time, t , by the reduced time. The relationship between t and t_r is usually expressed through shift factor parameter a_T as follows [39, 40]:

$$t_r = \int_0^t \frac{d\eta}{\alpha_T(\eta)} \quad (8)$$

Then, to determine a_T , Williams–Landel–Ferry empirical equation well-known as WLF equation is adopted with the following correlation.

$$\log_{10}(a_T) = \log_{10}\left(\frac{\tau(T)}{\tau(T_r)}\right) = -\frac{c_1(T(t)-T_r)}{c_2+(T(t)-T_r)} \quad (9)$$

where c_1 , c_2 and T_r are material constants and they together with Γ_∞ , Γ_i and τ_i can usually be calibrated by Dynamic Mechanical Thermal Analysis (DMTA) testing data. In this study, we use DMTA test data reported by Arrieta et al. [41] to calibrate thermo-time-dependent parameters. As a result, by replacing t with t_r in Eq. (6) or Eq. (7), the influence of thermal effect is considered. It is noted that the thermo-visco-hyperelastic contribution of the proposed model has been adopted by Westbrook et al. [42] and Diani and Arrieta [41, 43] and recently solved semi-analytically by Baniyadi et al. [39].

Here, to consider the electro-magnetic response of thermo-visco-hyperelastic materials, similar to recently proposed models [26, 28], we assume that the equilibrium part includes fibrous electro-magneto-hyperelastic behavior. Therefore, Eq. (7) can be reformulated as:

$$\boldsymbol{\sigma}(\mathbf{E}, \mathbf{H}, \boldsymbol{\varepsilon}, t) = \int_0^t \Gamma\left(t_r - \zeta_r\right) \frac{\partial \boldsymbol{\sigma}_{\text{FEHe}}}{\partial \zeta} d\zeta \quad (10)$$

where $\boldsymbol{\sigma}_{\text{FEHe}}$ is the stress depending on electric field, magnetic field, and mechanical strain which will be discussed in the next section.

2.2 Constitutive Equations for Fibrous Electro-Magneto-Responsive Polymers

2.2.1 Transversely isotropic hyperelastic materials

The transversely isotropic hyperelastic behavior of the incompressible material is defined using a single fiber family with angle of θ . Then, the unit vector of the anisotropy direction in the reference configuration is assumed to be \mathbf{A} . In this way, to obtain the total stress, invariants I_1 to I_5 are defined as [44]:

$$I_1 = \text{tr}(\mathbf{b}); I_2 = \frac{1}{2}(\text{tr}(\mathbf{b})^2 - \text{tr}(\mathbf{b}^2)); I_3 = \det(\mathbf{b}) = 1 \quad (11)$$

$$I_4 = \mathbf{FA} \cdot \mathbf{FA}; I_5 = \mathbf{F}^T \mathbf{a} \cdot \mathbf{F}^T \mathbf{a}$$

in which tr represents the symbol of trace. \mathbf{F} is the deformation gradient tensor, \mathbf{b} is the left Cauchy-Green tensor that is equal to \mathbf{FF}^T . Also, \mathbf{a} is the unit vector of the anisotropy direction in the current configuration and it is equal to \mathbf{FA} . It is noted that the fourth invariant presents the square of the stretch in the direction of \mathbf{A} . Then, based on the non-linear solid mechanics and utilizing the chain rule of differentiation, the Cauchy stress of fibrous hyperelastic materials, $\boldsymbol{\sigma}_{FH}$, is obtained in terms of the strain energy function as [45]:

$$\boldsymbol{\sigma}_{FH} = -p\mathbf{I} + \mathbf{F} \frac{\partial \Omega}{\partial \mathbf{F}} = -p\mathbf{I} + \mathbf{F} \sum_{i=1}^{i=5} \left(\frac{\partial \Omega}{\partial I_i} \frac{\partial I_i}{\partial \mathbf{F}} \right) \quad (12)$$

wherein \mathbf{I} and p are the second order identity tensor and hydrostatic parameter, respectively.

To calculate $\frac{\partial I_4}{\partial \mathbf{F}}$ and $\frac{\partial I_5}{\partial \mathbf{F}}$, we have the following relationship:

$$\frac{\partial I_4}{\partial \mathbf{F}} = 2\mathbf{A} \otimes \mathbf{FA}; \frac{\partial I_5}{\partial \mathbf{F}} = 2(\mathbf{A} \otimes \mathbf{FCA} + \mathbf{CA} \otimes \mathbf{FA}) \quad (13)$$

in which \mathbf{C} and \otimes represent the right Cauchy-Green tensor and outer product, respectively. Finally, based on non-linear solid mechanics and Eqs. (11)-(13), the general form of the Cauchy stress with the strain-energy density function in terms of $(I_1: I_5)$ for incompressible transversely hyperelastic materials by assuming perfect bonding between fibers and matrix is given by:

$$\boldsymbol{\sigma}_{FH} = -p\mathbf{I} + 2\Omega_1 \mathbf{b} + 2\Omega_2 (I_1 \mathbf{b} - \mathbf{b}^2) + 2\Omega_4 \mathbf{a} \otimes \mathbf{a} + 2\Omega_5 (\mathbf{a} \otimes \mathbf{ba} + \mathbf{ba} \otimes \mathbf{a}) \quad (14)$$

2.2.2 Electro-magneto-responsive polymers

In the electro-magneto-elasticity theory, the total Cauchy stress tensor is commonly derived by two approaches of superposition of purely elastic, electric, and magnetic stresses and using nominal Helmholtz free energy density function. The first approach by ignoring couple mechanical-electric and magnetic terms, is usually used for small strain deformation and eventually it may produce a remarkable error in the calculation of the total stress under large deformations [46-49]. Based on the first approach, the total Cauchy stress, $\boldsymbol{\sigma}_{EM}$, based on Maxwell's concept for electro-magneto-elastic materials can be expressed as [50]:

$$\boldsymbol{\sigma}_{EM} = \boldsymbol{\sigma}_{FH} + \boldsymbol{\tau}_p + \boldsymbol{\tau}_e + \boldsymbol{\tau}_m \quad (15)$$

where $\boldsymbol{\sigma}_{FH}$, $\boldsymbol{\tau}_p$, $\boldsymbol{\tau}_e$ and $\boldsymbol{\tau}_m$ are mechanical Cauchy stress, polarization stress tensor, electrostatic Maxwell stress tensor, and magnetic Maxwell stress tensor defined as [51, 52]:

$$\boldsymbol{\tau}_e = \varepsilon_0 \left[\mathbf{E} \otimes \mathbf{E} - \frac{1}{2} (\mathbf{E} \cdot \mathbf{E}) \mathbf{I} \right]; \boldsymbol{\tau}_m = \frac{1}{\mu_0} \left[\mathbf{B} \otimes \mathbf{B} - \frac{1}{2} (\mathbf{B} \cdot \mathbf{B}) \mathbf{I} \right]; \boldsymbol{\tau}_p = \mathbf{P} \otimes \mathbf{E} \quad (16)$$

in which \mathbf{E} , \mathbf{B} , \mathbf{P} , ε_0 and μ_0 are the electric field vector in the current configuration, magnetic induction vector in the current configuration, polarization density vector in the current configuration, electric permittivity of free space, and magnetic permeability of free space, respectively.

The second approach that considers the deformation dependency on the electric permittivity and the magnetic permeability, is an alternative and reliable method in electro-magneto-elasticity theory, in particular, at large strains [46-49]. In this way, many researchers have used different types of nominal Helmholtz free energy density functions such as Kumar and Sarangi [48, 49], Yarali et al. [28], and Dorfmann and Ogden [50, 53]. In this study, a nominal Helmholtz free energy density function in terms of deformation gradient tensor, electric field vector, and magnetic field vector introduced by Kumar and Sarangi [49] is adopted as:

$$\Omega(\mathbf{F}, \mathbf{H}^l, \mathbf{E}^l) = \rho \phi(\mathbf{F}, \mathbf{H}^l, \mathbf{E}^l) - \frac{1}{2} \varepsilon_0 \mathbf{E}^l \cdot (\mathbf{b}^{-1} \mathbf{E}^l) + \frac{1}{2\mu_0} \mathbf{B}^l \cdot (\mathbf{b} \mathbf{B}^l) \quad (17)$$

wherein \mathbf{H}^l , \mathbf{E}^l , ρ and \mathbf{B}^l represent the magnetic field in the reference configuration, electric field in the reference configuration, mass density in the current configuration, and magnetic induction vector in the reference configuration, respectively. Meanwhile, the correlation between electric and magnetic fields vectors in the reference and current configurations are expressed as $E^l = \mathbf{F}^T \mathbf{E}$ and $H^l = \mathbf{F}^T \mathbf{H}$, respectively. It is noted that quantities without superscript ' l ' represent those quantities in the current configuration.

In addition, the principal invariants depending on the tensor \mathbf{b} , \mathbf{E}^l and \mathbf{H}^l can be expressed as [49]:

$$\begin{aligned} I_6 &= (\mathbf{E}^l \otimes \mathbf{E}^l) : \mathbf{I}; I_7 = (\mathbf{E}^l \otimes \mathbf{E}^l) : \mathbf{b}^{-1}; I_8 = (\mathbf{E}^l \otimes \mathbf{E}^l) : \mathbf{b}^{-2} \\ I_9 &= (\mathbf{H}^l \otimes \mathbf{H}^l) : \mathbf{I}; I_{10} = (\mathbf{H}^l \otimes \mathbf{H}^l) : \mathbf{b}; I_{11} = (\mathbf{H}^l \otimes \mathbf{H}^l) : \mathbf{b}^2 \end{aligned} \quad (18)$$

wherein $:$ represents the symbol of double-contraction. In this study, it is assumed that the electric field and magnetic field are constant. Also, the direct coupling between the electric field and the magnetic field is ignored (*e.g.*, ignoring another invariant associating with both electric and magnetic fields). Analogous to Eq. (12), the total Cauchy stresses for electro-magneto elastomers can be expressed as [51]:

$$\boldsymbol{\sigma}_{EM} = -p\mathbf{I} + \mathbf{F} \frac{\partial \Omega}{\partial \mathbf{F}} = -p\mathbf{I} + \mathbf{F} \sum_{i=6}^{i=11} \left(\frac{\partial \Omega}{\partial I_i} \frac{\partial I_i}{\partial \mathbf{F}} \right) \quad (19)$$

Then, from Eqs. (18) and (19), the explicit form of $\boldsymbol{\sigma}_{EM}$ is obtained by performing some mathematical manipulation as:

$$\begin{aligned} \boldsymbol{\sigma}_{EM} = & -p\mathbf{I} - 2\Omega_7 \mathbf{E} \otimes \mathbf{E} - 2\Omega_8 (\mathbf{b}^{-1} \mathbf{E} \otimes \mathbf{E} + \mathbf{E} \otimes \mathbf{b}^{-1} \mathbf{E}) + \\ & 2\Omega_{10} \mathbf{bH} \otimes \mathbf{bH} + 2\Omega_{11} (\mathbf{bH} \otimes \mathbf{b}^2 \mathbf{H} + \mathbf{b}^2 \mathbf{H} \otimes \mathbf{bH}) \end{aligned} \quad (20)$$

where Ω_i ($i = 7:11$) = $\partial \Omega / \partial I_i$.

As a result, by considering both sections 2.2.1 and 2.2.2, the total Cauchy stress for fibrous electro-magneto-hyperelastic materials employing the chain rule of differentiation can be derived as:

$$\boldsymbol{\sigma}_{FEH\epsilon} = -p\mathbf{I} + \mathbf{F} \frac{\partial \Omega}{\partial \mathbf{F}} = -p\mathbf{I} + \mathbf{F} \sum_{i=1}^{i=11} \left(\frac{\partial \Omega}{\partial I_i} \frac{\partial I_i}{\partial \mathbf{F}} \right) \quad (21)$$

Finally, by integrating Eqs. (12), (14), (19), (20), and (21), the total Cauchy stress for fibrous electro-magneto-hyperelastic elastomers can be expressed as:

$$\begin{aligned} \boldsymbol{\sigma}_{FEH\epsilon} = & -p\mathbf{I} + 2\Omega_1 \mathbf{b} + 2\Omega_2 (I_1 \mathbf{b} - \mathbf{b}^2) + 2\Omega_4 \mathbf{a} \otimes \mathbf{a} + \\ & 2\Omega_5 (\mathbf{a} \otimes \mathbf{b} \mathbf{a} + \mathbf{b} \mathbf{a} \otimes \mathbf{a}) - 2\Omega_7 \mathbf{E} \otimes \mathbf{E} - 2\Omega_8 (\mathbf{b}^{-1} \mathbf{E} \otimes \mathbf{E} + \mathbf{E} \otimes \mathbf{b}^{-1} \mathbf{E}) + \\ & 2\Omega_{10} (\mathbf{bH} \otimes \mathbf{bH}) + 2\Omega_{11} (\mathbf{bH} \otimes \mathbf{b}^2 \mathbf{H} + \mathbf{b}^2 \mathbf{H} \otimes \mathbf{bH}) \end{aligned} \quad (22)$$

Therefore, by identifying and adopting a nominal Helmholtz free energy density function (*i.e.*, Ω) and deformation gradient tensor, total Cauchy stress for fibrous electro-magneto-hyperelastic elastomers can be calculated.

Here, by adopting the Neo-Hookean model for the purely mechanical hyperelastic property of the material, and based on the research works done in [28, 48, 50, 53, 54], a version of the nominal Helmholtz free energy density function for transversely isotropic electro-magneto-hyperelastic materials by ignoring the matrix-fiber interaction is considered as:

$$\Omega = C_1 (I_1 - 3) - \frac{\bar{E}}{2} q \ln \left(1 - \frac{(I_4 - 1)^2}{q} \right) + \frac{\epsilon_0}{2} (C_3 I_6 + C_4 I_7) + \frac{\mu_0}{2} (C_6 I_9 + C_7 I_{10}) \quad (23)$$

in which C_1 , C_3 , C_4 , C_6 and C_7 are materials constants. q is a positive non-dimensional parameter that measures the rapidly increasing stiffness of the fibers with increasing stretch [55], and \bar{E} is a positive material modulus that measures the degree of anisotropy.

Finally, by substituting Eq. (23) into Eq. (22), and consequent results in Eq. (10), the total Cauchy stress for TEMFSMPs is obtained. Thus, in this paper, we show that the proposed model can successfully be used for the SME of TEMFSMPs. In other words, by implementing the proposed model for a thermo-mechanical cycle of SMPs, we can get thermally-induced SME in the presence of electric and magnetic fields. To apply the model and solve the proposed constitutive equations, we need to discretize it which is detailed in the following section.

2.3 Time-Discretization of the Constitutive Equations for Thermo-Electro-Magneto-Responsive SMPs

Firstly, Eq. (10), by considering Eq. (5), at t^n in a generic time interval (t^{n-1}, t^n) is discretized as follows:

$$\boldsymbol{\sigma}^n = \int_0^{t^n} \left(1 - \sum_{i=1}^n \Gamma_i \left(1 - \exp\left(-\frac{t_r^n - \zeta_r}{\tau_i}\right) \right) \right) \frac{\partial \boldsymbol{\sigma}_{\text{FEH}\epsilon}}{\partial \zeta} d\zeta \quad (24)$$

Then, Eq. (24) can be rewritten in another form as:

$$\boldsymbol{\sigma}^n = \boldsymbol{\sigma}_{\text{FEH}\epsilon}^n - \sum_{i=1}^n \Gamma_i \boldsymbol{\sigma}_i^n \quad (25)$$

in which $\boldsymbol{\sigma}_i^n$ is

$$\boldsymbol{\sigma}_i^n = \boldsymbol{\sigma}_{\text{FEH}\epsilon}^n - \int_0^{t^n} e^{-\frac{t_r^n - \zeta_r}{\tau_i}} \frac{\partial \boldsymbol{\sigma}_{\text{FEH}\epsilon}}{\partial \zeta} d\zeta = \boldsymbol{\sigma}_{\text{FEH}\epsilon}^n - \Pi_i^n \quad (26)$$

where Π_i^n is expressed as:

$$\Pi_i^n = \int_0^{t^n} \exp\left(-\frac{t_r^n - \zeta_r}{\tau_i}\right) \frac{\partial \boldsymbol{\sigma}_{\text{FEH}\epsilon}}{\partial \zeta} d\zeta = \exp\left(-\frac{\Delta t_r^n}{\tau_i}\right) \Pi_i^{n-1} + \int_{t^{n-1}}^{t^n} \exp\left(-\frac{t_r^n - \zeta_r}{\tau_i}\right) \frac{\partial \boldsymbol{\sigma}_{\text{FEH}\epsilon}}{\partial \zeta} d\zeta \quad (27)$$

Since the time step from t^{n-1} to t^n is small, assuming a linear approximation for fibrous electro-magneto-hyperelastic stress variations in each time increment results in:

$$\boldsymbol{\sigma}^n = \boldsymbol{\sigma}_{\text{FEH}\epsilon}^n \left(1 - \sum_{i=1}^n \Gamma_i \right) + \sum_{i=1}^n \Gamma_i \left(\exp\left(-\frac{\Delta t_r^n}{\tau_i}\right) \Pi_i^{n-1} + \frac{\boldsymbol{\sigma}_{\text{FEH}\epsilon}^n - \boldsymbol{\sigma}_{\text{FEH}\epsilon}^{n-1}}{\Delta t^n} \int_{t^{n-1}}^{t^n} \exp\left(-\frac{t_r^n - \zeta_r}{\tau_i}\right) d\zeta \right) \quad (28)$$

Employing Eq. (28), the total stress in each time increment can be found using its corresponding value from the previous increment, while Π_i^{n-1} behaves like a history variable on the stress.

Then, since the WLF has an exponential form, its time-discretization is not straightforward and demands a high computational cost. To settle this issue, alternatively, we use a satisfying linear approximation as follows [39]:

$$h_T = -\ln(a_{T(t)}) = -\ln\left(10^{\frac{c_1(T(t)-T_r)}{c_2+(T(t)-T_r)}}\right) = \chi + \gamma t \quad (29)$$

$$a_{T(t)}^{-1} = \exp(\chi + \gamma t)$$

where parameters χ and γ are defined as:

$$\begin{aligned} \chi^n &= \frac{1}{\Delta t^n} (t^n h_T^{n-1} - t^{n-1} h_T^n) \\ \gamma^n &= \frac{1}{\Delta t^n} (h_T^n - h_T^{n-1}) \end{aligned} \quad (30)$$

Therefore, the reduced time at the current increment can be calculated through the previous increment and Eq. (30) as:

$$t_r^n = t_r^{n-1} + \int_{t^{n-1}}^{t^n} \exp(\chi + \gamma\eta) d\eta \quad (31)$$

3 A Non-Linear Continuum Framework for a Uniaxial Tension Problem

In this section, to implement and solve the proposed model, a uniaxial tension test is applied. In this regard, an incompressible visco-hyperelastic rectangular beam in the presence of thermal effect and uniaxial electric and magnetic fields is considered as shown in Figure 1.a. Cartesian coordinates (X, Y, Z) and (x, y, z) are employed for reference and current configurations, respectively. Both the electric and magnetic fields are applied in the X_1 direction with the magnitude of E_0 and H_0 , respectively. The mapping of a pure homogeneous deformation can be expressed as:

$$x_1 = \lambda_1 X_1 \quad x_2 = \lambda_2 X_2 \quad x_3 = \lambda_3 X_3 \quad (32)$$

where λ_i 's ($i=1:3$) are the principal stretches. Therefore, based on the definition of deformation gradient tensor in the Cartesian-Cartesian system and Eq. (32), the following equation can be obtained.

$$\mathbf{F} = \begin{bmatrix} \frac{\partial x}{\partial X} & \frac{\partial x}{\partial Y} & \frac{\partial x}{\partial Z} \\ \frac{\partial y}{\partial X} & \frac{\partial y}{\partial Y} & \frac{\partial y}{\partial Z} \\ \frac{\partial z}{\partial X} & \frac{\partial z}{\partial Y} & \frac{\partial z}{\partial Z} \end{bmatrix} = \begin{bmatrix} \lambda_1 & 0 & 0 \\ 0 & \lambda_2 & 0 \\ 0 & 0 & \lambda_3 \end{bmatrix} = \text{diag}(\lambda_1, \lambda_2, \lambda_3) \quad (33)$$

Then, by applying the assumption of incompressibility, we have $J_{\mathbf{F}_{\text{FEH}\epsilon}} = \det(\mathbf{F}_{\text{FEH}\epsilon}) = \lambda_1 \lambda_2 \lambda_3 = 1$. Consequently, for the uniaxial tension, we have $\lambda_1 = \lambda, \lambda_2 = \lambda_3 = \lambda^{-0.5}$ and eventually by employing Eq. (33), the deformation gradient tensor becomes equal to $\mathbf{F} = \text{diag}(\lambda, \lambda^{-0.5}, \lambda^{-0.5})$. In addition, based on the multiplicative decomposition of tensors, the total deformation gradient tensor can be decomposed into an electro-magneto-mechanical contribution $\mathbf{F}_{\text{FEH}\epsilon}$ and a purely thermal one \mathbf{F}_T as described in Eq. (34), which represents the Duhamel-Neumann hypothesis in the nonlinear deformation theory [56].

$$\mathbf{F} = \mathbf{F}_T \mathbf{F}_{\text{FEH}\epsilon}, \quad J = J_T J_{\text{FEH}\epsilon} \quad (34)$$

Since TEMFSMPs are assumed to be thermally isotropic, the deformation gradient \mathbf{F}_T can be given by a diagonal tensor as:

$$\mathbf{F}_T = F(T) \mathbf{I} \quad F(T) = \exp \left[\int_{T_0}^T \alpha(\hat{T}) d\hat{T} \right] = 1 + \int_{T_0}^T \alpha(T) dT = \Xi(T) \quad (35)$$

where $F(T)$ is a scalar function determining the thermal volume change, and $\alpha = \alpha(T)$ stands for the temperature-dependent thermal expansion coefficient. Then, by considering Eqs. (34) and (35), one may argue that $\mathbf{F}_{\text{FEH}\epsilon} = \mathbf{F} \mathbf{F}_T^{-1}$ resulting in:

$$\mathbf{F}_{\text{FEH}\epsilon} = \frac{1}{\Xi} \text{diag}(\lambda, \lambda^{-0.5}, \lambda^{-0.5}) \quad (36)$$

Besides, as mentioned before, the anisotropy vector in the reference configuration, electric and magnetic fields are defined as:

$$\mathbf{E} = (E_0, 0, 0); \mathbf{H} = (H_0, 0, 0); \mathbf{A} = (\sin(\theta), \cos(\theta), 0) \quad (37)$$

Subsequently, the left and right Cauchy-Green deformation tensors are derived as:

$$\mathbf{b} = \mathbf{C} = \frac{1}{\Xi^2} \text{diag}(\lambda^2, \lambda^{-1}, \lambda^{-1}) \quad (38)$$

Then, based on Eqs. (11) and (18), the invariants are obtained as:

$$\begin{aligned}
I_1 &= \frac{\lambda^3 + 2}{\lambda \Xi^2}, I_2 = \frac{2\lambda^3 + 1}{\lambda^2 \Xi^4}, I_3 = 1 \\
I_4 &= \frac{\lambda^3 \sin^2(\theta) + \cos^2(\theta)}{\lambda \Xi^2}; I_5 = \frac{\lambda^6 \sin^2(\theta) + \cos^2(\theta)}{\lambda^2 \Xi^4} \\
I_6 &= \frac{\lambda^2 E_0^2}{\Xi^2}; I_7 = E_0^2; I_8 = \frac{\Xi^2 E_0^2}{\lambda^2}; I_9 = \frac{\lambda^2 H_0^2}{\Xi^2}; I_{10} = \frac{\lambda^4 H_0^2}{\Xi^4}
\end{aligned} \tag{39}$$

Then, considering Eqs. (22) and (23), and $\sigma_{\text{FEH}\varepsilon_{22}} = \sigma_{\text{FEH}\varepsilon_{33}} = 0$, the hydrostatic parameter p can be found as:

$$p = \frac{2C_1}{\lambda \Xi^2} + \bar{E}q \frac{\Delta \cos^2(\theta)}{\lambda \Xi^2} \tag{40}$$

wherein the parameter Δ is defined as:

$$\Delta = \frac{\left(\frac{\lambda^2 \sin^2(\theta)}{\Xi^2} + \frac{\cos^2(\theta)}{\lambda \Xi^2} - 1 \right)}{\left(-\frac{\lambda^2 \sin^2(\theta)}{\Xi^2} - \frac{\cos^2(\theta)}{\lambda \Xi^2} + q + 1 \right)} \tag{41}$$

Finally, the uniaxial stress is obtained as:

$$\sigma_{\text{FEH}\varepsilon_{11}} = C_1 \left(\frac{2\lambda^3 - 2}{\lambda \Xi^2} \right) - \frac{\Delta \bar{E}q}{\lambda \Xi^2} \left(\frac{\cos^2(\theta) - \lambda^3 \sin^2(\theta)}{\lambda \Xi^2} \right) - \varepsilon_0 C_4 E_0^2 + \frac{\mu_0 C_7 \lambda^4 H_0^2}{\Xi^4} \tag{42}$$

Then, to eliminate material parameters, Eq. (42) is non-dimensionalized as:

$$\sigma_{\text{FEH}\varepsilon_{11}}^* = \left(\frac{2\lambda^3 - 2}{\lambda \Xi^2} \right) - \frac{\Delta \eta q}{\lambda \Xi^2} \left(\frac{\cos^2(\theta) - \lambda^3 \sin^2(\theta)}{\lambda \Xi^2} \right) + E_0^{*2} + \frac{\lambda^4 H_0^{*2}}{\Xi^4} \tag{43}$$

in which $\sigma_{\text{FEH}\varepsilon_{11}}^* = \sigma_{\text{FEH}\varepsilon_{11}}/C_1$, $\eta = \bar{E}/C_1$, $E_0^* = E_0 \sqrt{\varepsilon_0 C_4/C_1}$, and $H_0^* = H_0 \sqrt{\mu_0 C_7/C_1}$. Finally, by substituting Eq. (43) into Eq. (10), the total Cauchy stress for TEMFSMPs is obtained. As mentioned before, the material parameters associated with viscous part are adopted from Arrieta et al. [41] for an acrylate-based SMP.

As shown in Figure 1.d, the sample during the loading step is first deformed at a high temperature (*i.e.*, T_h), and then it is cooled down to a low temperature (*i.e.*, T_L) by maintaining the constraints applied during the previous stage. Next, the unloading process is performed by removing the mentioned constraints at T_L . Then, at the latest step, the sample is reheated up to retrieve its initial state so that it can recover both stored force and/or shape so-called *fixed-strain stress recovery* and *stress-free strain recovery*, respectively.

4 Results and Discussions

In this section, the results of the proposed model under uniaxial tension and torsion-extension loading regimes are presented. For this purpose, the proposed model under those loading regimes are solved semi-analytically using Maple software package (ver. 2018). Sections 4.1 and 4.2 represent the results of the model under uniaxial tension and simultaneous torsion and extension loadings, respectively.

4.1 Uniaxial tension loading

In section 4.1.1, the results for pure SMPs (*i.e.*, thermally-responsive SMPs without fibers in the absence of electric and magnetic fields) under the uniaxial tension are presented. In addition, the proposed semi-analytical solution is verified by experimental data reported in [41]. In section 4.1.2, the influence of fibers (*e.g.*, direction and stiffness of fibers) on the SME is investigated. In sections 4.1.3-4.1.5, the effects of purely electric field, purely magnetic field, and electro-magnetic fields are studied, respectively.

4.1.1 Thermally-Responsive Pure SMPs

In this section, in the absence of electric and magnetic fields, a thermo-mechanical cycle of the pure SMP without fibers is studied. 20% axial strain with 0.0018 s^{-1} strain rate is applied to an SMP specimen to stretch it. The temperature is varied from 25°C to 65°C (or vis versa) with $\frac{5^\circ\text{C}}{\text{min}}$ temperature rise rate. The problem is solved for both *stress-free strain recovery* and *fixed-strain stress recovery* cases to show shape memory recovery and recovery force of the pure SMP while being triggered by heat, respectively. Meanwhile, it should be mentioned that the thermo-mechanical cycle applied here is composed of four steps, see Figure 2:

- I. Step ① (Loading): applying 20% axial strain at high temperature, T_h .
- II. Step ② (Cooling): decreasing the temperature of the SMP from T_h to low temperature, T_l , while the strain is kept fixed.
- III. Step ③ (Unloading): the strain constraint is removed at T_l .
- IV. Step ④ (Heating): increasing temperature of the SMP from T_l to T_h for two different purposes: i. shape memory recovery (4s in Figure 2) and ii. recovery force (4f in Figure 2).

The results presented in Figure 2 show that there is a good correlation between experimental data [41] and the results from the present semi-analytical solution verifying the accuracy of the solution. It is noted that for all of the simulations in this study, we consider

$T_l = 25^\circ\text{C}$, $T_h = 65^\circ\text{C}$ and 20% axial strain with 0.0018 s^{-1} strain rate, except for studies presented in Figure 4.e and f and Figure 5.c.

4.1.2 *Thermally-Responsive Fibrous SMPs*

In this section, to reinforce pure SMPs, fibers are embedded into the matrix. As mentioned before, one of the disadvantages of thermally-responsive SMPs is the softening effect during the recovery step. It means that by increasing the temperature of the SMP, it becomes much softer and eventually restricts its applications for soft robotics and manipulators. To settle this issue, fibrous SMPs are introduced and the effects of fiber's orientation and stiffness are discussed in detail (see Figure 3).

Firstly, the influence of fiber's direction on the recovery force and shape memory recovery is investigated as shown in Figure 3.a and b, respectively. It is noted that θ is defined as the angle between fibers' direction and transverse direction of the tensile specimen. When fibers are parallel to the longitudinal direction of the specimen, maximum reinforcement can be achieved compared to other angles. Figure 3.a reveals that, while pure SMPs and SMP composites with $\theta = 0^\circ$ and 30° have an increasing trend of the stress recovery versus the temperature, a decreasing-increasing trend is seen for SMP composites with $\theta = 45^\circ$, 60° and 90° . It is directly related to the strong effect of the fiber reinforcement on the composite thermal expansion and its overall stiffness. It is seen that the SMP produces small and large negative compressive stresses for these two cases by initial heating due to the thermal expansion effect. Extra heating activates the programmed SMP composite and produces a positive stress recovery that makes the compressive stress faded, see Figure 3.a. It is found that the positive tensile stress recovery finally becomes dominant. From the shape memory recovery point of view, Figure 3.b shows that fibers do not have a significant effect on the strain recovery of the SMP that is in agreement with the conclusion drawn in Ref. [24]. It is observed that, by increasing the fiber's orientation (from the perpendicular state to the parallel state), the strain recovery path shifts to right. It means that at a specific temperature, the temporary shape is recovered more at the perpendicular state compared to the parallel state.

Next, the effect of fiber's stiffness is illustrated in Figure 3.c and d. From Figure 3.c, it is found that selecting stiffer fibers leads to larger final stress recovery. Regarding the strain recovery, a trend similar to the trend of the fiber orientation is seen, so that increasing the

stiffness of fibers shifts the strain recovery graph to right. It means that using stiffer fibers leads to a lower strain recovery at a specific temperature lower than 65° , see Figure 3.d.

Since one of the main motivations of this study is the improvement of the recovery force of SMPs, the stress recovery ratio for different fiber's orientation and stiffness is presented in Figure 3.e. Axial stress recovery ratio is defined as $\frac{\sigma_{11}^{*FSMP} - \sigma_{11}^{*PSMP}}{\sigma_{11}^{*PSMP}} \times 100$ in which σ_{11}^{*PSMP} and σ_{11}^{*FSMP} represent non-dimensional axial stresses for pure SMP and fibrous SMP, respectively. It is interestingly found that, for example, using fibers with $\eta = 10$ and $\theta = \pi/2$ results in a significant increase in the axial stress recovery ratio of about 640%. It is also seen that the maximum axial stress recovery ratio occurs when $\eta = 30$ and $\theta = \pi/2$ are selected.

4.1.3 Thermo-Electro-Responsive Fibrous SMPs

In this section, the effect of the purely electric field on thermally-responsive fibrous SMPs with $\eta = 10$ and $\theta = \pi/2$ is demonstrated in Figure 4.a and b. As shown in a recent research work [28], in the presence of the electric field, the material becomes stiffer. As can be seen in Figure 4.a, by increasing the non-dimensional electric field from 0 to 1.5, the final non-dimensional axial stress recovery increases by 5.5 times which makes the SMP more suitable for robotics applications where large forces are required. Regarding the strain recovery as investigated in Figure 4.b, two interesting phenomena can be observed. Firstly, it is found that under a high electric field, a shrinkage may occur in the specimen. This could enhance the applicability of SMPs for some specific applications such as biomedical stents with expanding and shrinking features. In fact, after a full shape memory recovery, by extra heating, the specimen becomes shorter and this feature could be exploited for removal purposes in biomedical applications. Secondly and more interestingly, through the electric field, the working temperature of the SMP is decreased which is an amazing achievement of the present modeling. For example, at non-dimensional electric field of 1.5, the SMP fully retrieves at 55.9°C , while the SMP in the absence of electric field is recovered at temperature of 65°C . This phenomenon makes SMPs more bio-applicable. As mentioned before, one of the main challenges in the application of SMPs for biomedical devices is their working temperature. In this study, for the first time, the electric field effect is exploited to reduce the SMP working temperature. In this way, working temperature reduction upon purely electric or magnetic field is presented in Figure 4.e. By interpolating the working temperature

reduction in terms of external purely electric field, one may obtain a relation $\Delta T_{Electric} = 1/1000(98 + 7812E_0^* - 1165E_0^{*2})$.

4.1.4 Thermo-Magneto-Responsive Fibrous SMPs

Considering Figure 4.c and d, it is seen that the purely magnetic field has an effect like the effect of the purely electric field on the stress recovery, but it is more significant. This is due to the effect of the stress induced by the magnetic field and boosted by the stretch term that results in a prominent influence on the stress recovery compared to the single applied electric field (see Eq. (43)). For example, it is found that applying non-dimensional magnetic field of 1.5 increases the non-dimensional axial stress recovery 11.22 times. This also reduces the working temperature to 56.7°C when a fully shape recovery happens. It can be concluded that the magnetic field like the electric field reduces the working temperature of the SMP and additionally makes a shrinkage in the specimen. However, the electric field with the same magnitude of the magnetic field results in a little lower working temperature and a larger shrinkage, see Figures 4.b and d. Besides, by considering Figure 4.e and by interpolating the working temperature reduction upon purely magnetic field, one may obtain a relation $\Delta T_{Magnetic} = 1/100(1 + 753H_0^* - 135H_0^{*2})$. As can be seen, while the single electric and magnetic fields reduce the working temperature in an almost linear manner until a non-dimensional field of 2, their effects become less beyond it and a saturation state may happen.

4.1.5 Thermo-Electro-Magneto-Responsive Fibrous SMPs

In this section, the coupling effect of electric and magnetic fields on the SME of TEMFSMPs is studied as shown in Figure 5. Considering Figure 5.a, it can be found that the coupled electro-magnetic field has the most influence on reinforcing SMPs compared to either purely electric or magnetic field. For example, the non-dimensional axial stress recovery of the SMP under non-dimensional purely electric field 1 is 0.069 and becomes 0.096 under non-dimensional purely magnetic field 1, while at the coupled non-dimensional electric and magnetic fields 1 and 1, the stress recovery increases to 0.105 that is larger than those induced under pure fields. Furthermore, as discussed in section 4.4 and based on Eq. (43), it is found that the effect of the electric field on the strain recovery and working temperature reduction is more significant than the magnetic field effect, see Figure 5.b.

In order to investigate the effect of the applied strain and the strain rate, a full thermo-mechanical cycle of the stress is demonstrated in Figure 5.c for 50% axial strain and strain

rate of 0.01 s^{-1} . The preliminary conclusion drawn from this figure is that the stress changes nonlinearly versus time during the mechanical loading stage that is due to the effect of high strain rate. As can be seen, by changing the coupled electric and magnetic fields, the axial stress can be tailored and increased significantly. For example, at $(E_0^*, H_0^*) = (4,4)$, the stress recovery of the TEMVHSMP can be enhanced by 2.5 times. The maximum stress (in the absolute sense) occurs when $(E_0^*, H_0^*) = (4,4)$ are applied. In addition, since one of the interesting achievements of this study is reducing the working temperature, a case study of how coupled electro-magnetic field may affect the working temperature is presented in Figure 5.d. By interpolating the working temperature reduction in terms of coupled electro-magnetic field, one may obtain the following relation:

$$\Delta T_{\text{Coupled}} = \frac{1}{1000} \left(-5 + 5635H_0^* + 6099E_0^* - 3375E_0^*H_0^* + 101E_0^{*2}H_0^{*2} \right) \quad (44)$$

where $\Delta T_{\text{Coupled}}$ represents the working temperature reduction induced by the coupled electro-magnetic field. Finally, a summary of results on the effect of fibers and electro-magnetic field on the axial stress recovery ratio is presented in Table 1 that can be useful as benchmark results for future numerical and experimental developments.

4.2 Complex loading regimes

The proposed model is general and is a 3D model which could be used in general and complex loading regimes. To investigate the ability of the model in complex and 3D loading regime, here we aim to present the potential of the developed model in torsion-extension of a cylinder. Torsion-extension loading of cylinders is one of the complex loading regime which can be used for the applications of sensors and biomedicine. Therefore, by considering the deformation gradient tensor for torsion-extension loading and applying boundary conditions, the total stress components, axial force and moment can be obtained. In this way, the deformation gradient tensor, \mathbf{F} and left Cauchy-Green tensor, \mathbf{b} of such deformation can be expressed as follows [26, 57, 58]:

$$\mathbf{F} = \begin{bmatrix} \gamma^{-1/2} & 0 & 0 \\ 0 & \gamma^{-1/2} & \beta\gamma^{1/2}R \\ 0 & 0 & \gamma \end{bmatrix}; \mathbf{b} = \mathbf{F}\mathbf{F}^T = \begin{bmatrix} \gamma^{-1} & 0 & 0 \\ 0 & \gamma^{-1} + \beta^2\lambda R^2 & \beta\lambda^{3/2}R \\ 0 & \beta\lambda^{3/2}R & \gamma^2 \end{bmatrix} \quad (45)$$

wherein γ and β are axial stretch and the amount of pitch per stretched length unit, respectively. Also, by applying uni-axial electric and magnetic fields, the anisotropy vector in the reference configuration, electric and magnetic fields are defined as:

$$\mathbf{E} = (0, 0, E_0); \mathbf{H} = (0, 0, H_0); \mathbf{A} = (0, \sin(\theta), \cos(\theta)) \quad (46)$$

After determining the total stress components, the total axial force and total moment can be determined by:

$$\begin{aligned} M &\equiv \int_0^{2\pi} \int_0^{r_0} \sigma_{z\theta} r^2 dr d\theta' = \int_0^{2\pi} \int_0^{\gamma^{-1/2}R_0} \gamma^{-3/2} \sigma_{Z\Theta} R^2 dR d\Theta \\ N &\equiv \int_0^{2\pi} \int_0^{r_0} \sigma_{zz} r dr d\theta' = \int_0^{2\pi} \int_0^{\gamma^{-1/2}R_0} \gamma^{-1} \sigma_{ZZ} R dR d\Theta \end{aligned} \quad (47)$$

where (r, θ', z) and (R, Θ, Z) are the current and reference coordinate system in cylindrical coordinates, respectively. Finally, by non-dimensionalizing the equations of the torsion-extension of a cylinder, the recovery moment/ recovery pitch angle and axial recovery force/ axial recovery strain under $\pi/4$ pitch angle and 20% axial strain through 100 s, are shown in Figure 6.a and b, respectively. From the stiffening phenomenon, it could be conducted that under the coupled electro-magnetic fields, the cylinder becomes stiffer. For instance, the recovery moment or axial force under $(E_0^*, H_0^*) = (0.5, 1.5)$ are almost three times larger than those in the absence of external fields. However, from the shape recovery perspective, we see that the axial recovery is more sensitive to external fields than torsional recovery. It means that the shrinkage effect can only be appeared in axial deformations not torsional deformation. However, it should be noted that since the external field are applied longitudinally, therefore, the torsional deformation is not expected to change dramatically. In addition, by considering the axial recovery strain, Figure 5.b, the temperature reduction can be seen upon increasing the uniaxial longitudinal electro-magnetic fields.

Meanwhile, by applying $\gamma=1$, in the case of simple torsion, the moment and pitch angle by considering fibers with $\eta = 10$ and $\theta = \pi/2$ under $\pi/2$ pitch angle through 100 s, are shown in Figure 6.c. As mentioned before, due to the direction of the external field applied to the cylinder, we do not expect to have a remarkable change in the pitch angle while being triggered by electro-magnetic fields. Unlike the pitch angle, the moment has a significant change upon the external field (*i.e.*, stiffening effect). It is due to the fact that by such a condition, some electric and magnetic-dependent term are included in $\sigma_{\theta z}$ and then in turn, in the moment.

5 Conclusion

The aim of this work was to model a new class of SMPs so-called thermo-electro-magneto-responsive fibrous SMPs with highly enhanced shape memory recovery and

recovery force and reduced working temperature. The 3D constitutive model was derived for TEMFSMPs based on the non-linear electro-magneto-visco-hyperelasticity theory. The semi-analytical solution was then developed for the cases of the tensile deformation and simultaneous torsion and extension loading. The accuracy of the model and the solution was validated via the comparative study with experimental results available in the literature for thermally-responsive pure SMPs. The detailed analysis of the influence of some parameters such as purely electric field, purely magnetic field, electro-magnetic fields, the stiffness of fibers, and their orientation was carried out. Numerical results revealed that the electro-magnetic field, the orientation and stiffness of fibers can effectively be set to tune the shape memory effect and bio-applicability of TEMFSMPs with highly enhanced stress/strain recovery and reduced working temperature.

Due to the absence of similar results and constitutive models in the specialized literature, this paper is likely to pave the way for designing advanced SMP devices for mechanical, biomedical and aerospace applications where large recovery force and lower working temperatures (*e.g.*, body temperature) are desirable. The model is expected to be an appropriate computational tool for design and analysis of advanced structures like adaptive soft grippers and biomedical stents with enhanced shape memory recovery and recovery force.

Conflict of Interest

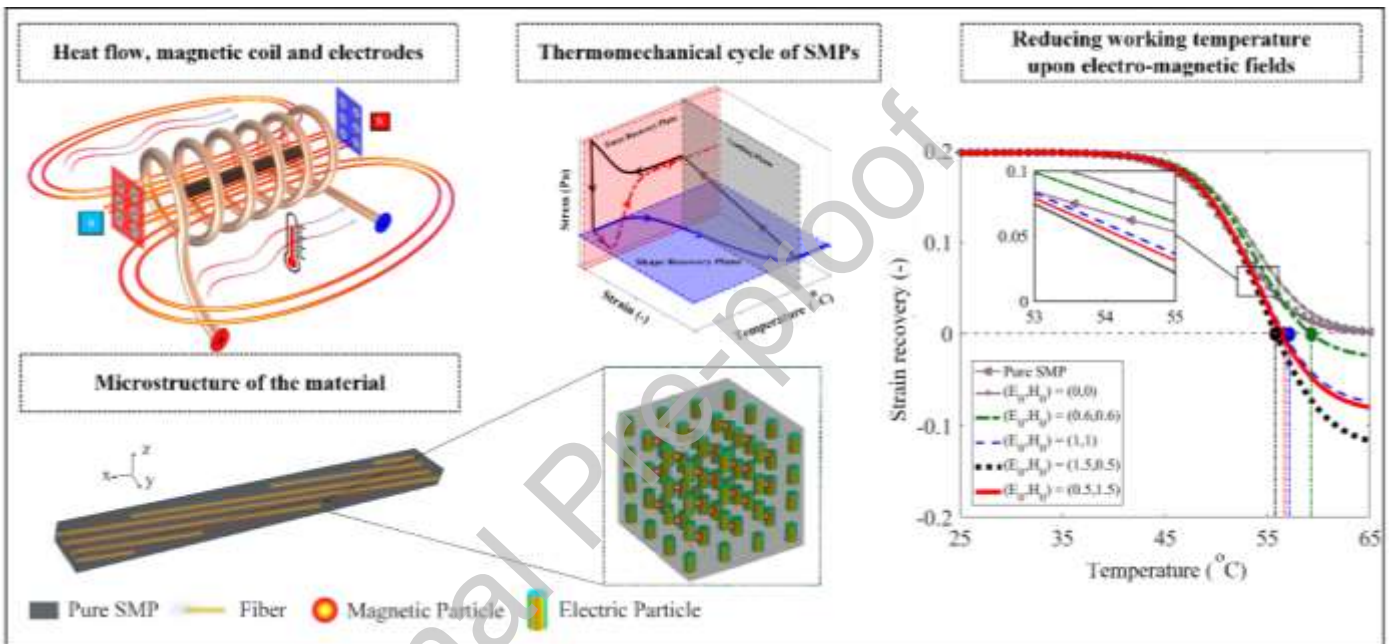
We confirm that there are no known conflicts of interest associated with this publication and there has been no significant financial support for this work that could have influenced its outcome.

Author Statement

Conceptualization, modeling, simulations, data collection and analysis: M. Baniasadi, E. Yarali; methodology: M. Baniasadi, E. Yarali, M. Bodaghi, A. Zolfagharian, M. Baghani; project administration: M. Bodaghi; supervision and technical advice: M. Bodaghi, A. Zolfagharian, M. Baghani; writing—original draft: M. Baniasadi, E. Yarali, M. Bodaghi;

writing—review & editing: M. Baniasadi, E. Yarali, M. Bodaghi, A. Zolfagharian; all authors have read and approved the current version of the paper; all authors have approved the order of authors listed in the paper.

Graphical Abstract



References

1. T. Xie, *Tunable polymer multi-shape memory effect*. Nature, 2010. **464**(7286): p. 267.
2. M. Tian, W. Gao, J. Hu, X. Xu, N. Ning, B. Yu, and L. Zhang, *Multi-directional triple shape memory polymer by tunable crosslinking and crystallization*. ACS Applied Materials & Interfaces, 2020.
3. M. Bodaghi and W. Liao, *4D printed tunable mechanical metamaterials with shape memory operations*. Smart Materials and Structures, 2019. **28**(4): p. 045019.
4. M. Baniassadi, A. Foyouzat, and M. Baghani, *Multiple Shape Memory Effect for Smart Helical Springs with Variable Stiffness over Time and Temperature*. International Journal of Mechanical Sciences, 2020. **182**: p. 105742.
5. N. Roudbarian, M. Baghani, M. Baniassadi, D. George, and A. Mohammadi, *An experimental investigation on the energy storage in a shape-memory-polymer system*. Energy Equipment and Systems, 2019. **7**(4): p. 309-316.
6. K. Yu, Y. Liu, and J. Leng, *Conductive shape memory polymer composite incorporated with hybrid fillers: electrical, mechanical, and shape memory properties*. Journal of Intelligent Material Systems and Structures, 2011. **22**(4): p. 369-379.
7. X. Wan, F. Zhang, Y. Liu, and J. Leng, *CNT-based electro-responsive shape memory functionalized 3D printed nanocomposites for liquid sensors*. Carbon, 2019.
8. T. Li, Y. Li, X. Wang, X. Li, and J. Sun, *Thermally and Near-Infrared Light-Induced Shape Memory Polymers Capable of Healing Mechanical Damage and Fatigued Shape Memory Function*. ACS applied materials & interfaces, 2019. **11**(9): p. 9470-9477.
9. J. ZHANG, Y. BAI, and X. CHEN, *Development of light-induced shape memory polymers*. SCIENTIA SINICA Technologica, 2020.
10. S.-Y. Gu, S.-P. Jin, X.-F. Gao, and J. Mu, *Poly lactide-based polyurethane shape memory nanocomposites (Fe₃O₄/PLAUs) with fast magnetic responsiveness*. Smart Materials and Structures, 2016. **25**(5): p. 055036.
11. P. Testa, R.W. Style, J.Z. Cui, C. Donnelly, E. Borisova, P.M. Derlet, E.R. Dufresne, and L.J. Heyderman, *Magnetically Addressable Shape-Memory and Stiffening in a Composite Elastomer*. Advanced Materials, 2019. **31**(29): p. 6.
12. A. Melocchi, N. Inverardi, M. Uboldi, F. Baldi, A. Maroni, S. Pandini, F. Briatico-Vangosa, L. Zema, and A. Gazzaniga, *Retentive device for intravesical drug delivery based on water-induced shape memory response of poly (vinyl alcohol): design concept and 4D printing feasibility*. International journal of pharmaceutics, 2019. **559**: p. 299-311.
13. C. Yan, Q. Yang, and G. Li, *A phenomenological constitutive model for semicrystalline two-way shape memory polymers*. International Journal of Mechanical Sciences, 2020: p. 105552.
14. M. Ahmad, J. Luo, B. Xu, H. Purnawali, P.J. King, P.R. Chalker, Y. Fu, W. Huang, and M. MirafTAB, *Synthesis and characterization of polyurethane-based shape-memory polymers for tailored T_g around body temperature for medical applications*. Macromolecular Chemistry and Physics, 2011. **212**(6): p. 592-602.
15. K. Yu, Y. Liu, and J. Leng, *Shape memory polymer/CNT composites and their microwave induced shape memory behaviors*. Rsc Advances, 2014. **4**(6): p. 2961-2968.
16. L. Yahia, *Shape memory polymers for biomedical applications*. 2015: Elsevier.
17. M. Baniassadi, E. Yarali, A. Foyouzat, and M. Baghani, *Crack self-healing of thermo-responsive shape memory polymers with application to control valves, filtration, and*

- drug delivery capsule*. European Journal of Mechanics - A/Solids, 2021. **85**: p. 104093.
18. G. Tandon, J. Baur, and A. McClung, *Shape Memory Polymers for Aerospace Applications: Novel Synthesis, Modeling, Characterization and Design*. 2015: DEStech Publications, Inc.
 19. A. Bruni, F.G. Serra, A. Deregibus, and T. Castroflorio, *Shape-Memory Polymers in Dentistry: Systematic Review and Patent Landscape Report*. Materials, 2019. **12**(14): p. 2216.
 20. W. Zhao, L. Liu, F. Zhang, J. Leng, and Y. Liu, *Shape memory polymers and their composites in biomedical applications*. Materials Science and Engineering: C, 2019. **97**: p. 864-883.
 21. M. Bodaghi, A. Serjouei, A. Zolfagharian, M. Fotouhi, H. Rahman, and D. Durand, *Reversible energy absorbing meta-sandwiches by FDM 4D printing*. International Journal of Mechanical Sciences, 2020. **173**: p. 105451.
 22. E. Yarali, A. Taheri, and M. Baghani, *A comprehensive review on thermomechanical constitutive models for shape memory polymers*. Journal of Intelligent Material Systems and Structures, 2020: p. 1045389X20916795.
 23. I. Niyonzima, Y. Jiao, and J. Fish, *Modeling and simulation of nonlinear electro-thermo-mechanical continua with application to shape memory polymeric medical devices*. Computer Methods in Applied Mechanics and Engineering, 2019. **350**: p. 511-534.
 24. E. Yarali, M. Baniassadi, and M. Baghani, *Numerical homogenization of coiled carbon nanotube reinforced shape memory polymer nanocomposites*. Smart Materials and Structures, 2019. **28**(3): p. 035026.
 25. M. Abbasi-Shirsavar, M. Baghani, M. Taghavimehr, M. Golzar, M. Nikzad, M. Ansari, and D. George, *An experimental–numerical study on shape memory behavior of PU/PCL/ZnO ternary blend*. Journal of Intelligent Material Systems and Structures, 2018. **30**(1): p. 116-126.
 26. E. Yarali, M. Baniassadi, M. Bodaghi, and M. Baghani, *3D constitutive modeling of electro-magneto-visco-hyperelastic elastomers: a semi-analytical solution for cylinders under large torsion–extension deformation*. Smart Materials and Structures, 2020. **29**(8): p. 085031.
 27. E. Yarali, A. Mohammadi, S. Mafakheri, M. Baghani, and H. Adibi, *Mathematical modeling and experimental evaluation of a prototype double-tube Magnetorheological damper*. SN Applied Sciences, 2019. **1**(11): p. 1341.
 28. E. Yarali, R. Noroozi, A. Yousefi, M. Bodaghi, and M. Baghani, *Multi-Trigger Thermo-Electro-Mechanical Soft Actuators under Large Deformations*. Polymers, 2020. **12**(2): p. 489.
 29. A. Rossi, F. Orsini, A. Scorza, F. Botta, N.P. Belfiore, and S.A. Sciuto. *A review on parametric dynamic models of magnetorheological dampers and their characterization methods*. in *Actuators*. 2018. Multidisciplinary Digital Publishing Institute.
 30. S.-t. Xing, P.-p. Wang, S.-q. Liu, Y.-h. Xu, R.-m. Zheng, Z.-f. Deng, Z.-f. Peng, J.-y. Li, Y.-y. Wu, and L. Liu, *A shape-memory soft actuator integrated with reversible electric/moisture actuating and strain sensing*. Composites Science and Technology, 2020: p. 108133.
 31. H. Zeng, J. Leng, J. Gu, and H. Sun, *Modeling the thermomechanical behaviors of short fiber reinforced shape memory polymer composites*. International Journal of Mechanical Sciences, 2020. **166**: p. 105212.

32. W. Zhang, F. Zhang, X. Lan, J. Leng, A.S. Wu, T.M. Bryson, C. Cotton, B. Gu, B. Sun, and T.-W. Chou, *Shape memory behavior and recovery force of 4D printed textile functional composites*. Composites Science and Technology, 2018. **160**: p. 224-230.
33. Y. Liu, W. Zhang, F. Zhang, J. Leng, S. Pei, L. Wang, X. Jia, C. Cotton, B. Sun, and T.-W. Chou, *Microstructural design for enhanced shape memory behavior of 4D printed composites based on carbon nanotube/polylactic acid filament*. Composites Science and Technology, 2019. **181**: p. 107692.
34. N. Roudbarian, M. Baniasadi, M. Ansari, and M. Baghani, *An experimental investigation on structural design of shape memory polymers*. Smart Materials and Structures, 2019. **28**(9): p. 095017.
35. F. Zhang, L. Wang, Z. Zheng, Y. Liu, and J. Leng, *Magnetic programming of 4D printed shape memory composite structures*. Composites Part A: Applied Science and Manufacturing, 2019. **125**: p. 105571.
36. T. Calvo-Correas, A. Shirole, F. Crippa, A. Fink, C. Weder, M.A. Corcuera, and A. Eceiza, *Biocompatible thermo- and magneto-responsive shape-memory polyurethane bionanocomposites*. Materials Science and Engineering: C, 2019. **97**: p. 658-668.
37. H. Khajehsaeid, J. Arghavani, R. Naghdabadi, and S. Sohrabpour, *A visco-hyperelastic constitutive model for rubber-like materials: A rate-dependent relaxation time scheme*. International Journal of Engineering Science, 2014. **79**: p. 44-58.
38. H.F. Brinson and L.C. Brinson, *Polymer engineering science and viscoelasticity*. New York: Springer, 2008. **66**: p. 79.
39. M. Baniasadi, M.-A. Maleki-Bigdeli, and M. Baghani, *Force and multiple-shape-recovery in shape-memory-polymers under finite deformation torsion-extension*. Smart Materials and Structures, 2020. **29**(5): p. 055011.
40. P. Fan, W. Chen, B. Zhao, J. Hu, J. Gao, G. Fang, and F. Peng, *Formulation and numerical implementation of tensile shape memory process of shape memory polymers*. Polymer, 2018.
41. S. Arrieta, J. Diani, and P. Gilormini, *Experimental characterization and thermoviscoelastic modeling of strain and stress recoveries of an amorphous polymer network*. Mechanics of materials, 2014. **68**: p. 95-103.
42. K.K. Westbrook, P.H. Kao, F. Castro, Y. Ding, and H.J. Qi, *A 3D finite deformation constitutive model for amorphous shape memory polymers: a multi-branch modeling approach for nonequilibrium relaxation processes*. Mechanics of Materials, 2011. **43**(12): p. 853-869.
43. J. Diani, P. Gilormini, C. Frédy, and I. Rousseau, *Predicting thermal shape memory of crosslinked polymer networks from linear viscoelasticity*. International Journal of Solids and Structures, 2012. **49**(5): p. 793-799.
44. C.O. Horgan and J.G. Murphy, *Extension or Compression Induced Twisting in Fiber-Reinforced Nonlinearly Elastic Circular Cylinders*. Journal of Elasticity, 2016. **125**(1): p. 73-85.
45. A.G. Holzapfel, *Nonlinear Solid Mechanics II*. 2000.
46. X. Zhao and Z. Suo, *Electrostriction in elastic dielectrics undergoing large deformation*. Journal of Applied Physics, 2008. **104**(12): p. 123530.
47. C. Rinaldi and H. Brenner, *Body versus surface forces in continuum mechanics: Is the Maxwell stress tensor a physically objective Cauchy stress?* Physical Review E, 2002. **65**(3): p. 036615.
48. D. Kumar, S. Sarangi, and P. Saxena, *Universal relations in coupled electro-magneto-elasticity*. Mechanics of Materials, 2020. **143**: p. 103308.

49. D. Kumar and S. Sarangi, *Electro-magnetostriction under large deformation: modeling with experimental validation*. Mechanics of Materials, 2019. **128**: p. 1-10.
50. A. Dorfmann and R. Ogden, *Nonlinear electroelasticity*. Acta Mechanica, 2005. **174**(3-4): p. 167-183.
51. L. Dorfmann and R.W. Ogden, *Nonlinear theory of electroelastic and magnetoelastic interactions*. 2014: Springer.
52. N. Cohen, K. Dayal, and G. deBotton, *Electroelasticity of polymer networks*. Journal of the Mechanics and Physics of Solids, 2016. **92**: p. 105-126.
53. A. Dorfmann and R. Ogden, *Nonlinear magnetoelastic deformations*. Quarterly Journal of Mechanics and Applied Mathematics, 2004. **57**(4): p. 599-622.
54. C.O. Horgan and G. Saccomandi, *A new constitutive theory for fiber-reinforced incompressible nonlinearly elastic solids*. Journal of the Mechanics and Physics of Solids, 2005. **53**(9): p. 1985-2015.
55. C.O. Horgan and M.G. Smayda, *An anisotropic nonlinear elasticity model for tearing of fibrous soft biomaterials*. Mathematics and Mechanics of Solids, 2013. **18**(6): p. 607-621.
56. E. Yarali, R. Noroozi, A. Moallemi, A. Taheri, and M. Baghani, *Developing an analytical solution for a thermally tunable soft actuator under finite bending*. Mechanics Based Design of Structures and Machines, 2020: p. 1-15.
57. C.O. Horgan and J.G. Murphy, *Extension and torsion of incompressible non-linearly elastic solid circular cylinders*. Mathematics and Mechanics of Solids, 2011. **16**(5): p. 482-491.
58. M. Baniasadi, P. Fareghi, F. Darijani, and M. Baghani, *Finite strain relaxation and creep in coupled axial and torsional deformation*. Mechanics Based Design of Structures and Machines, 2020: p. 1-17.

List of Figures

Figure 1. Overall schematic drawing of the present problem including (a) a specimen in the presence of the electric field, magnetic field and thermal flow; (b) a tensile specimen and its microstructure containing electric and magnetic particles and fibers; (c) a schematic of the working temperature reduction in TEMFSMPs compared to pure SMPs; (d) a thermo-mechanical cycle applied to the tensile specimen.

Figure 2. A thermo-mechanical cycle of a thermally-responsive pure SMP (*i.e.*, without fibers) for both shape memory recovery and recovery force cases with 20% axial strain and strain rate of 0.0018 s^{-1} : model predictions versus experimental data [41].

Figure 3. The effect of the fiber angle, θ and ratio of stiffness of the fiber and SMP matrix, η on (a and c) non-dimensional axial stress recovery and (b and d) axial strain recovery under zero electric and magnetic fields; (e) The variation of the axial stress recovery ratio versus different fiber angles and fiber stiffness in the absence of electric and magnetic fields under 20% axial strain and strain rate of 0.0018 s^{-1} . It is noted that while changing θ , $\eta = 10$ is kept fixed and while changing η , $\theta = \pi/2$ is kept fixed.

Figure 4. The effect of the purely electric and magnetic fields on (a and c) non-dimensional axial stress recovery and (b and d) axial strain recovery with $\eta = 10$ and $\theta = \pi/2$ under 20% axial strain and strain rate of 0.0018 s^{-1} ; the variation of the temperature reduction under the (e) coupled electro-magnetic fields with $\eta = 10$ and $\theta = \pi/2$ for 0.01 s^{-1} strain rate and 50% axial strain.

Figure 5. The effect of the electro-magnetic fields on (a) non-dimensional axial stress recovery and (b) axial strain recovery with $\eta = 10$ and $\theta = \pi/2$ under 20% axial strain and strain rate of 0.0018 s^{-1} ; (c) the variation of the non-dimensional axial stress and (d) the temperature reduction under the coupled electro-magnetic fields with $\eta = 10$ and $\theta = \pi/2$ for 0.01 s^{-1} strain rate and 50% axial strain.

Figure 6. The effect of the coupled electro-magnetic fields on (a) non-dimensional recovery moment and recovery pitch angle (b) axial recovery strain and recovery force under torsion-extension loading of a cylinder at 20% axial strain through 100 s and $\pi/4$ torsion angle (c) moment and pitch angle of a cylinder under simple torsion with $\eta = 10$ and $\theta = \pi/2$ under $\pi/2$ torsion angle.

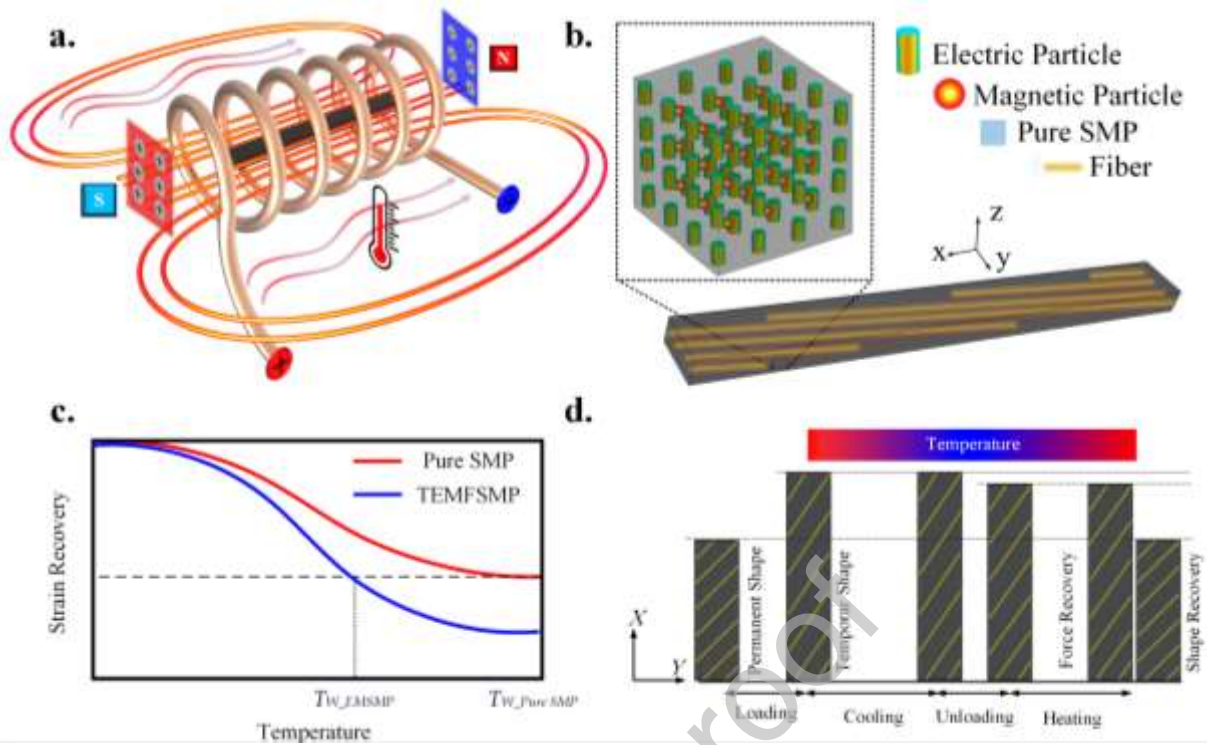


Figure 1. Overall schematic drawing of the present problem including (a) a specimen in the presence of the electric field, magnetic field and thermal flow; (b) a tensile specimen and its microstructure containing electric and magnetic particles and fibers; (c) a schematic of the working temperature reduction in TEMFSMPs compared to pure SMPs; (d) a thermo-mechanical cycle applied to the tensile specimen.

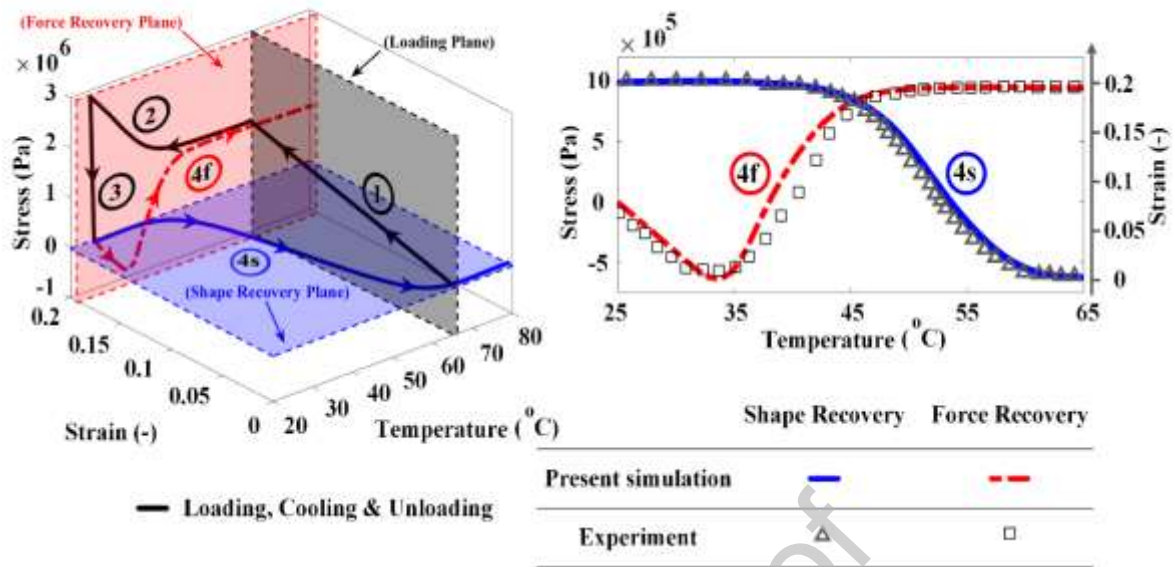


Figure 2. A thermo-mechanical cycle of a thermally-responsive pure SMP (*i.e.*, without fibers) for both shape memory recovery and recovery force cases with 20% axial strain and strain rate of 0.0018 s^{-1} : model predictions versus experimental data [41].

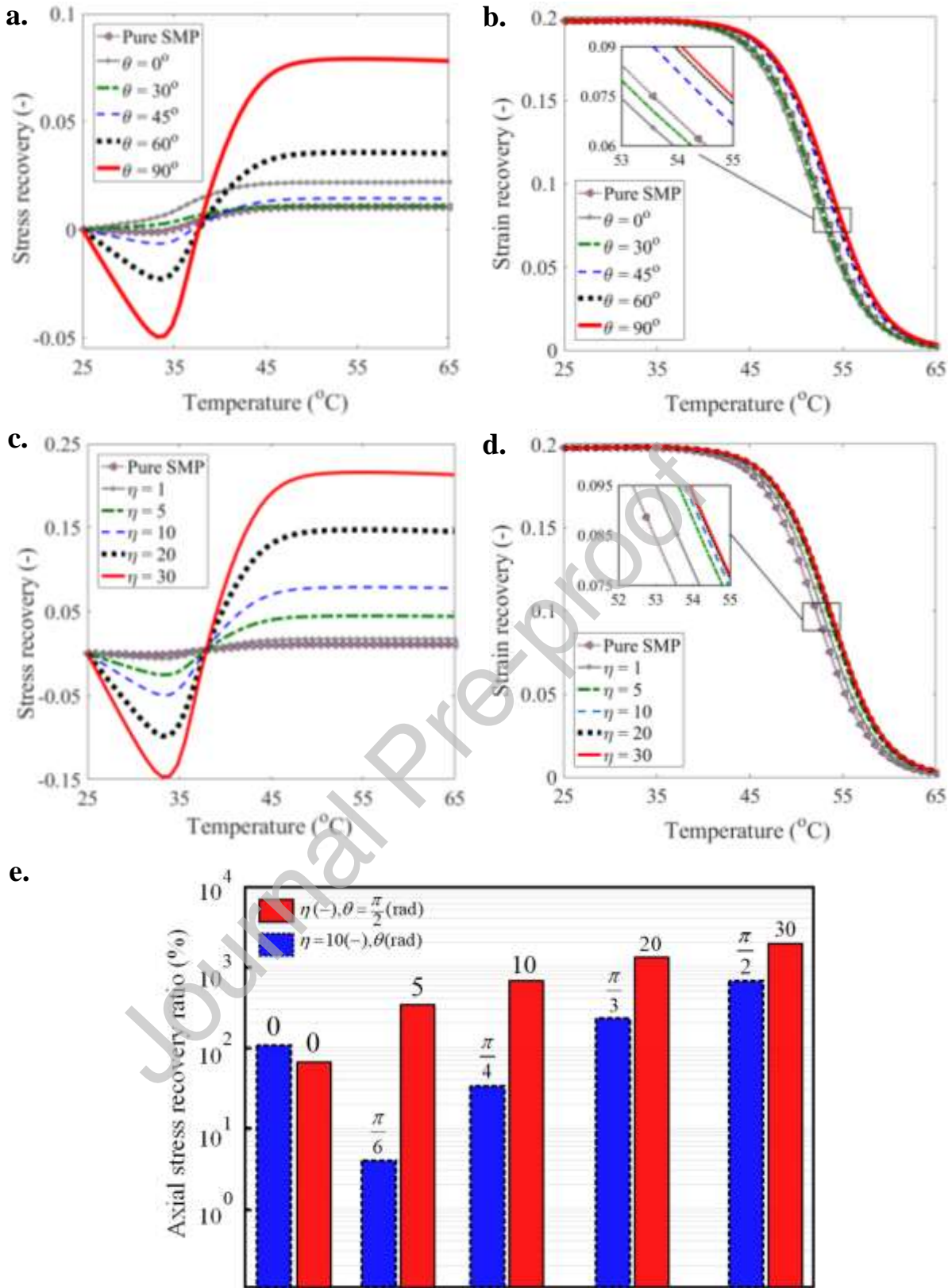


Figure 3. The effect of the fiber angle, θ and ratio of stiffness of the fiber and SMP matrix, η on (a and c) non-dimensional axial stress recovery and (b and d) axial strain recovery under zero electric and magnetic fields; (e) the variation of the axial stress recovery ratio versus different fiber angles and fiber stiffness in the absence of electric and magnetic fields under

20% axial strain and strain rate of 0.0018 s^{-1} . It is noted that while changing θ , $\eta = 10$ is kept fixed and while changing η , $\theta = \pi/2$ is kept fixed.

Journal Pre-proof

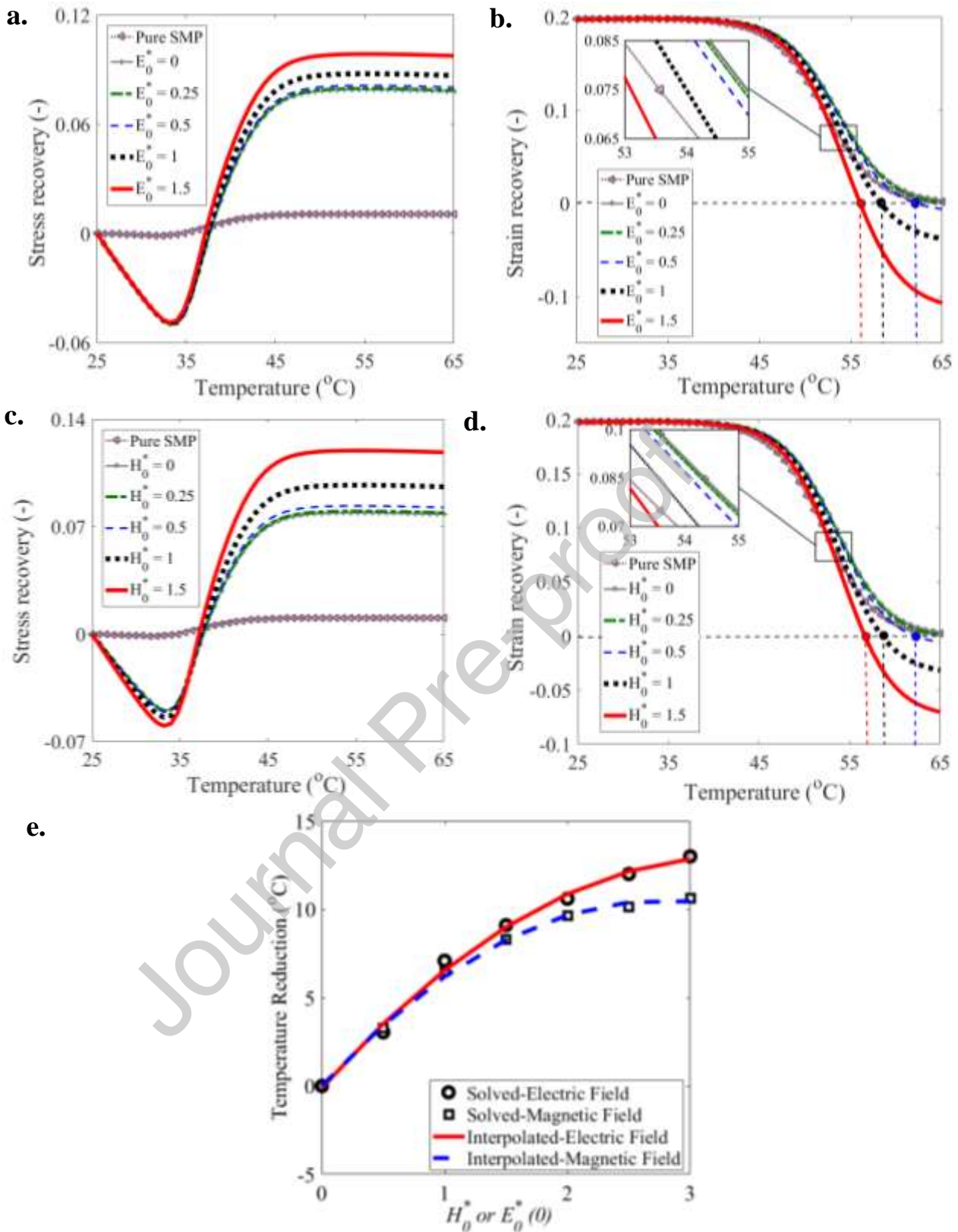


Figure 4. The effect of the purely electric and magnetic fields on (a and c) non-dimensional axial stress recovery and (b and d) axial strain recovery with $\eta = 10$ and $\theta = \pi/2$ under 20% axial strain and strain rate of 0.0018 s^{-1} ; the variation of the temperature reduction under the (e) coupled electro-magnetic fields with $\eta = 10$ and $\theta = \pi/2$ for 0.01 s^{-1} strain rate and 50% axial strain.

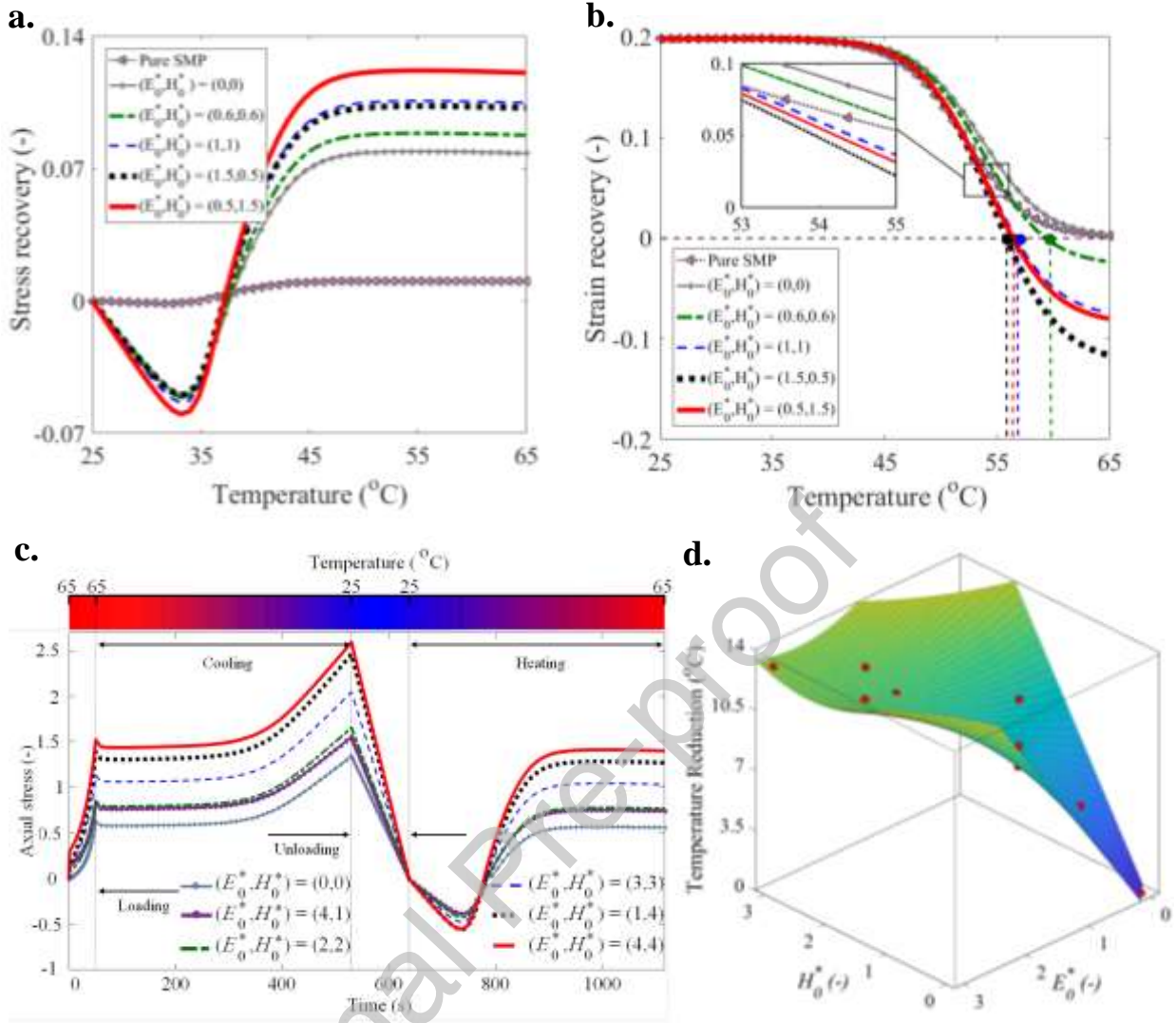


Figure 5. The effect of electro-magnetic fields on (a) non-dimensional axial stress recovery and (b) axial strain recovery with $\eta = 10$ and $\theta = \pi/2$ under 20% axial strain and strain rate of 0.0018 s^{-1} ; (c) the variation of the non-dimensional axial stress and (d) the temperature reduction under the coupled electro-magnetic fields with $\eta = 10$ and $\theta = \pi/2$ for 0.01 s^{-1} strain rate and 50% axial strain

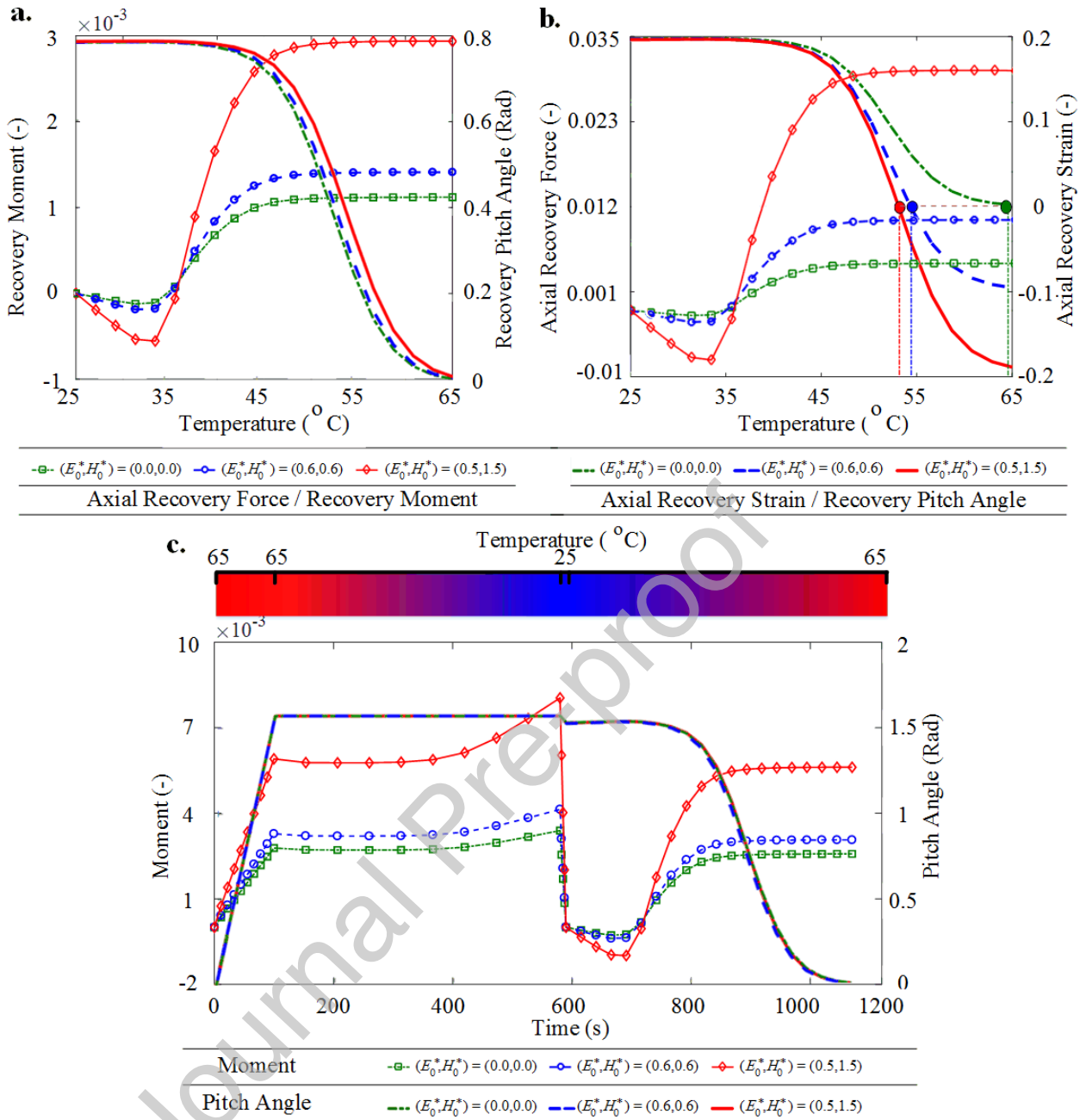


Figure 6. The effect of the coupled electro-magnetic fields on (a) non-dimensional recovery moment and recovery pitch angle (b) axial recovery strain and recovery force under torsion-extension loading of a cylinder at 20% axial strain through 100 s and $\pi/4$ torsion angle (c) moment and pitch angle of a cylinder under simple torsion with $\eta = 10$ and $\theta = \pi/2$ under $\pi/2$ torsion angle.

List of Table

Table 1. Variation of the axial stress recovery ratio with different parameters E_0^* , H_0^* , η and θ under $T_l = 25^\circ C$, $T_h = 65^\circ C$ and 20% axial strain with 0018 s^{-1} strain rate.

Journal Pre-proof

Table 1. Variation of the axial stress recovery ratio with different parameters E_0^* , H_0^* , η and θ under $T_l = 25^\circ\text{C}$, $T_h = 65^\circ\text{C}$ and 20% axial strain with 0.0018 s^{-1} strain rate.

The coupling between electric and magnetic fields with $\eta= 10$ and $\theta = \pi/2$		
E_0^* (-)	H_0^* (-)	Stress Recovery Ratio (%)
0	0	0
0.6	0.6	12.29
1.5	0.5	30.78
1	1	34.13
0.5	1.5	54.54
The variations of θ and η in the absence of electric and magnetic fields		
η	θ	Stress Recovery Ratio (%)
0	90	0
1	90	63.96
5	90	319.80
10	0	108.00
	30	3.80
	45	35.58
	60	233.97
	90	639.60
20	90	1279.20
30	90	1918.8